Int. J. Heat Mass Transfer. Vol. 32, No. 9, pp. 1697–1708, 1989
Printed in Great Britain

0017-9310/89 $3.00+0.00

Study of local natural convection heat transfer in an inclined enclosure

F. J. HAMADY and J. R. LLOYD
Department of Mechanical Engineering, Michigan State University, East Lansing, MI 48824, U.S.A.

and

H. Q. YANG and K. T. YANG
Department of Aerospace and Mechanical Engineering, University of Notre Dame, Notre Dame, IN 46556, U.S.A.

(*Received* 23 *December* 1987 *and in final form* 2 *February* 1989)

Abstract—The effect of inclination on the steady natural convection local heat transfer characteristics in an air-filled differentially heated enclosure with cross-sectional aspect ratio one is studied experimentally and numerically. Measurements of local and mean Nusselt numbers are obtained at various inclination angles, ranging between 0° (heated from above) and 180° (heated from below), for Rayleigh numbers between 10^4 and 10^6 and are compared with the numerical predictions. The heat flux at the hot and cold boundaries show strong dependence on the angle of inclination and the Rayleigh number. In addition, new results and details are made available concerning the local heat transfer distributions as a function of the inclination angle and Rayleigh number. Flow patterns, stream functions and isotherms at different inclination angles are shown in order to give new insight and greater understanding of the flow and heat transfer behavior.

INTRODUCTION

THIS WORK is a combined experimental and numerical study of the influence of inclined boundaries and Rayleigh number on the local natural convection heat transfer in an air-filled differentially heated enclosure. In a variety of engineering applications enclosures are inclined to the direction of gravity which results in the need to consider the effects of both the tangential and normal components of the buoyancy force relative to the differentially heated walls. At large inclination angles the effect of the component of buoyancy normal to the heated surface becomes very important in modifying both the flow structure and the heat transfer.

The importance of the inclined convection problem is pointed out in the review papers by Ostrach [1], Catton [2] and quite recently, by Raithby and Hollands [3]. Until about 1970 there had been little consideration given to the effects of inclined boundaries on thermal convection or to the effect of inclusion of parameters such as the enclosure aspect ratio or the angle of inclination. Most of the studies performed on different aspects of the subject were very limited. During that time an excellent work was conducted by Hart [4], who used both analytical and experimental procedures to reveal the significant features of the effect of enclosure inclination between the two limiting cases, Bénard convection (heated from below) and convection in a vertical slot, however, no measurements of local heat transfer were performed.

Recent developments pointed to the need of a more comprehensive treatment of the subject. Ayyaswamy and Catton [5] analytically considered the fluid flow in a differentially heated inclined rectangular cavity, and developed a correlation for the average Nusselt number in terms of the average Rayleigh number and the angle of inclination. Later, Catton *et al.* [6] applied the Galerkin method to analyze the natural convection flow of a large Prandtl number fluid at various inclination angles. The method was used, in the case of the Boussinesq approximation, for Rayleigh numbers up to 2×10^5 and aspect ratios between 0.1 and 20.

Hollands and Konicek [7, 8] studied the various flow regimes in terms of the range of values of the critical Rayleigh numbers closely related to the stability of the horizontal, vertical and inclined air layers. Their results for the measured critical Rayleigh numbers are in close agreement with the work reported by Unny [9], and through their experimental analysis the principal modes of flow were discussed. For the horizontal mode (Bénard problem), the instability is associated with what may be called a 'top-heavy' situation. Heat is transferred by conduction across the fluid layer, when the Rayleigh number is less than the critical ($Ra_c < 1708$) value, while for the inclined layer two types of instabilities should be considered, the static top-heavy, and the gravitational buoyancy associated with the vertical slot. The relative magnitude of the influence of each depends on the angle of inclination, and at the critical angle which was

NOMENCLATURE

A_x aspect ratio, (height/width)
A_z longitudinal aspect ratio, (length/width)
C_p specific heat at constant pressure [J kg^{-1} K^{-1}]
g gravitational acceleration [m s^{-2}]
Gr Grashof number, $g\beta H^3(T_H - T_C)/\nu^2$
H enclosure height ($H = W$) [m]
h convective heat transfer coefficient [W m^{-2} K^{-1}]
k thermal conductivity [W m^{-1} K^{-1}]
L length of the enclosure [m]
Nu local Nusselt number, see equation (8)
$\overline{Nu}$ mean Nusselt number, see equation (9)
P static pressure [Pa]
Pr Prandtl number, ν/α
Ra Rayleigh number, $g\beta H^3(T_H - T_C)/\alpha\nu$
T temperature [°C]
t time [s]
u, v, w velocity components in the x-, y-, z-directions [m s^{-1}]
W enclosure width [m]
x, y, z coordinates in the x-, y-, z-directions.

Greek symbols
α thermal diffusivity [m^2 s^{-1}]
β volumetric thermal expansion coefficient [K^{-1}]
δ_{ij} Kronecker delta
ζ non-dimensional distance along the x-direction, x/H
θ non-dimensional temperature, $(T - T_C)/(T_H - T_C)$
θ_0 non-dimensional wall temperature difference, $(T_R - T_C)/T_C$
μ dynamic viscosity [kg m^{-1} s^{-1}]
ν kinematic viscosity [m^2 s^{-1}]
ρ density [kg m^{-3}]
σ_{ij} stress tensor
Φ dissipation function [s^{-2}]
ϕ inclination angle between the cold surface and the horizontal direction [deg.].

Subscripts
a air
C cold surface
H hot surface
i, j, k coordinate indices
m mean
R reference
s surface.

Superscript
$\bar{}$ dimensional quantity.

determined by Hart to be 162° and by Unny to be 168° where a transition from one mode into another can be seen. Another interesting experimental analysis across an inclined air layer was also developed by Hollands *et al.* [10]. The Rayleigh number considered is from subcritical to 10^5 and the angle of inclination between 180° and 110°. Under these conditions their correlation predicted excellent agreement with the experimental data points. In this experimental line Elshirbiny *et al.* [11, 12] conducted an extensive study to examine the influence of the angle of inclination and the aspect ratio on the heat transfer rate. A set of correlations was obtained to calculate the Nusselt number which is of great importance in the applications of windows and solar collectors, where free convection constitutes the main mode of the heat loss.

In a series of papers Ozoe *et al.* [13–16] carried out experimental and numerical studies in inclined enclosures with different thermal boundary conditions and aspect ratios. Their studies were thoroughly conducted and provided valuable information concerning flow patterns, velocities and temperature distributions. The overall heat transfer measurements followed quite well what would be anticipated based on the observed flow patterns.

Arnold *et al.* [17] conducted an extensive experimental study of the influence of the inclination angle and the aspect ratio on the average heat transfer rate. Their results indicated that for a small aspect ratio the local minimum in mean Nusselt number becomes more pronounced and occurs closer to 180° (heated from below). This in turn suggests that the unicell and the cellular motion do not superpose. In general, their results showed reasonable agreement with those of Ozoe *et al.*

Some of the recent contributions to the basic aspects of analysis of natural convection in inclined enclosures, were the introduction of variable properties in the numerical methods and the establishment of the limits of validity of the Boussinesq approximation. Zhong *et al.* [18] and Yang *et al.* [19] have applied their numerical analysis to a study of the effects of variable thermal properties, thermal conductivity, viscosity and heat capacity. In their work flow patterns and heat transfer were analyzed for a complete set of inclination angles. Conductive heat transfer was found to dominate the heat transfer for inclination angles ranging from 0° (heated from above) to 45°. For larger angles, convection was the prevailing heat transfer mode, due to the apparent increase of the gravitational effect along the differentially heated walls. Transitions from unicell to

three-dimensional oblique rolls have been seen at critical angles between 150° and 180°, and are accompanied by a local minimum in the heat transfer rate. Moreover, their correlation for the mean Nusselt number based on fully variable properties compared favorably with the results of refs. [5, 17].

Although papers in this field are still appearing [20–23] it would seem that much is yet to be learned about the effects of inclined boundaries and their impact on the local heat transfer distribution. It was clear from the survey prepared for this study that a substantial amount of theoretical and experimental work has been conducted to improve our understanding of the fundamental aspects of heat transfer in enclosures. However, local Nusselt number distributions have not received such detailed attention. Accordingly the present study will focus on the effect of inclining the boundaries on the local Nusselt number distributions for various Rayleigh numbers. In addition, a visual study of the hydrodynamic and thermal boundary layers is established to provide new insight and physical interpretation of the flow and heat transfer in the vicinity of the heated walls.

MATHEMATICAL FORMULATION

Figure 1 shows the geometry of a three-dimensional rectangular enclosure. The surfaces at $y = 0$ and H are differentially heated with the cold surface at $y = 0$, and all the other surfaces are insulated. Aspect ratios which define the relative dimensions of the enclosure are $A_x = W/H = 1$ and $A_z = L/H = 10$. The working fluid is air. The equations governing the three-dimensional laminar natural convection process in enclosures are the conservation equations of mass, momentum and energy. The following definitions are used to make the equations dimensionless:

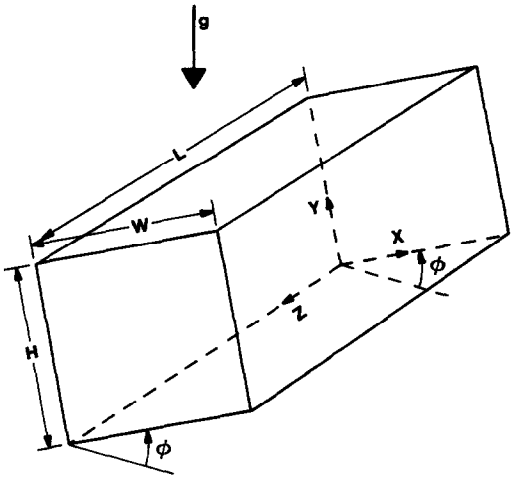

FIG. 1. Geometry of the three-dimensional inclined rectangular enclosure.

$$x_i = \frac{\bar{x}_i}{H}, \quad t = \frac{\bar{t}u_R}{H}, \quad g_i = \frac{\bar{g}_i H}{u_R^2}$$

$$u_i = \frac{\bar{u}_i}{u_R}, \quad T = \frac{\bar{T}}{T_R}, \quad p = \frac{\bar{p}}{\rho_R u_R^2}$$

$$\rho = \frac{\bar{\rho}}{\rho_R}, \quad c_{pm} = \frac{\bar{c}_{pm}}{c_{pR}}, \quad \mu = \frac{\bar{\mu}}{\rho_R u_R H}, \quad k = \frac{\bar{k}}{\rho_R c_{pm} u_R H} \tag{1}$$

where all barred quantities are dimensional, subscript R refers to reference quantities, and $i = 1, 2, 3$. In the above equations, $\bar{x}_i$ are the rectangular coordinates, $\bar{t}$ the time variable, $\bar{g}_i$ the gravitational acceleration vector, $\bar{u}_i$ the velocity vector, $\bar{T}$ the temperature, $\bar{p}$ the static pressure, $\bar{\rho}$ the fluid density, $\bar{c}_{pm}$ the fluid mean specific heat, μ the fluid viscosity, and $\bar{k}$ the fluid thermal conductivity. The governing conservation equations can now be written in dimensionless tensor form as follows:

$$\rho_{,t} + (\rho u_i)_{,i} = 0 \tag{2}$$

$$(\rho u_i)_{,t} + (\rho u_i u_j)_{,j} = -P_{,i} - \rho g_i + \sigma_{ij,j} \tag{3}$$

$$(\rho c_{pm} T)_{,t} + (\rho u_i c_{pm} T)_{,j} = (kT_{,i})_{,i} + \mu\Phi - pu_{i,i} \tag{4}$$

where subscript t denotes derivatives with respect to time. Furthermore, the dimensionless shear stress tensor σ_{ij}, specific heat c_{pm} and dissipation function Φ are in turn given by

$$\sigma_{ij} = \mu(u_{i,j} + u_{j,i} - \tfrac{2}{3}\delta_{ij}u_{k,k}) \tag{5}$$

$$c_{pm} = \frac{1}{T-1}\int_1^T c_p \, dT \tag{6}$$

$$\Phi = 2u_{i,i}^2 + [u_{ij}(1-\delta_{ij})]^2 - \tfrac{2}{3}u_{i,i}^2 \tag{7}$$

respectively, δ_{ij} is the Kronecker delta. The variations of μ, k and c_p as functions of temperature are in accordance with those utilized in ref. [18], where it was concluded that the Boussinesq approximation for the enclosure problems is certainly valid when $\theta_0 \leqslant 0.1$. At $\theta_0 = 0.2$ and $Ra = 10^6$, the Boussinesq approximation still predicts the correct Nusselt number within 2%, even though the vertical velocity components may be over-estimated by as much as 20%. The reference velocity u_R is chosen to be 0.3048 m s^{-1}, and ρ_R and c_{pR} are evaluated at the cold wall temperature. Accordingly, the Boussinesq approximation is not invoked in the present study.

The governing equations are discretized by the control volume approach which insures the conservative characteristics to be satisfied in every cell and the whole calculation domain. In this study the QUICK (quadratic upstream interpolation for convection kinematics) scheme, originally suggested by Leonard [24], is extended to three-dimensional calculations. This scheme has been shown to give good accuracy and stability [15], and details of the solution procedure can be found in ref. [25].

Most numerical studies which have been performed on enclosure problems have heretofore assumed that the insulated surface as found in the experiments are

adiabatic. A few have also looked at the perfect conductor limit also. In the present study the actual experimental boundary conditions are input to the numerical analysis. The thermocouple readings for the hot and cold surfaces were averaged (less than 1°C variation was measured) and the average value was used as T_H or T_C. For the insulated surfaces, the thermocouple readings were used to specify the temperature of the insulated wall. Since the thermocouples were in the plastic their locations were noted and conduction through the plastic walls was accounted for in the numerical code. This presents a unique opportunity to compare the experimental and calculated temperature and flow fields with the same boundary conditions existing in both the experimental and numerical studies.

EXPERIMENTAL APPARATUS AND PROCEDURE

The experimental apparatus is displayed in Fig. 2. The test section consists of two vertical aluminum plates and two horizontal plexiglas plates which are contained inside the rotating frame. The aluminum plates are 50.80 cm square and 2.54 cm thick. The channels for water circulation from both the hot and cold constant temperature baths are, 1.27 cm wide and 1.27 cm deep and are milled into the back sides of the aluminum plates. The use of aluminum of high thermal conductivity, and the channel design to act as a counter flow heat exchanger were intended to balance out possible temperature gradients and to maintain isothermal working surfaces. The plates were polished to a smooth finish of 25 μm flatness. The plexiglas plates are 5.08 cm wide, 50.80 cm long and 1.27 cm thick. The edges are milled at 60° to keep a very small contact area with the isothermal plates, thereby reducing conduction. The test section is carefully covered with layers of fiberglass insulation 7.0 cm thick to reduce the heat loss. The inside dimensions of the enclosure are 5.08 cm × 5.08 cm × 50.80 cm. High quality optical glass, accurate to one-tenth of a wavelength (green light), and 2.54 cm thick were installed at the front and back faces of the test section for interferometric measurements, and they were covered with removable rubber foam to facilitate photographic and visual observations.

Eighteen copper–constantan thermocouples were installed in both the hot and cold plates. The junctions were cemented into small holes drilled into the back side approximately 3.0 mm from the front surface. In particular, the apparatus was designed and made so that all the fine adjustments could be performed before any test began. A more detailed description of the experimental set-up is given in ref. [26].

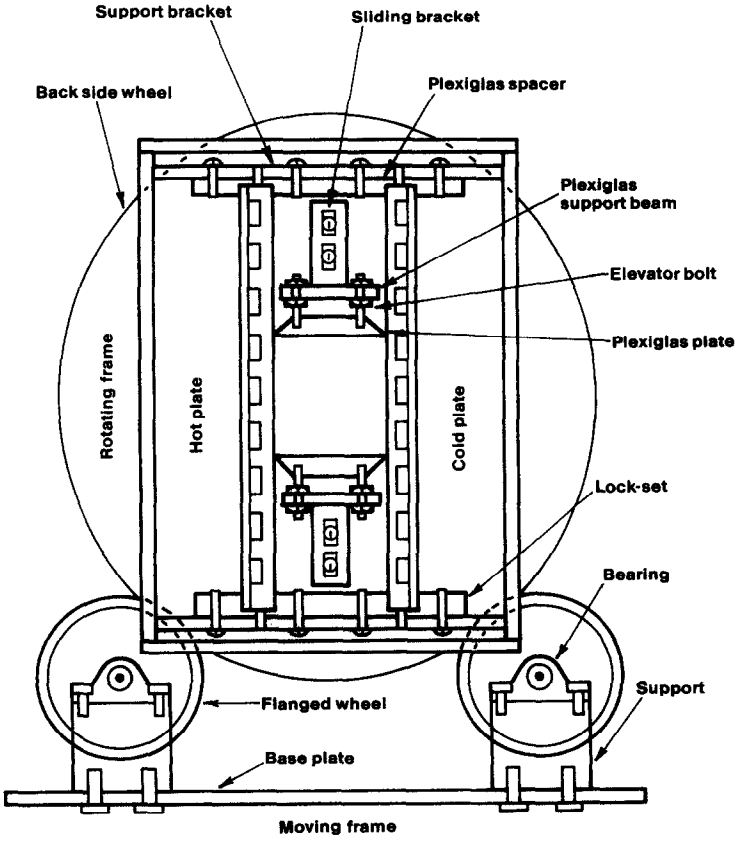

FIG. 2. Schematic diagram of the experimental apparatus.

In this study a Mach–Zhender interferometer was employed to reveal the entire temperature field, and subsequently to enable the measurement of the local and mean Nusselt numbers along the heated surfaces. In addition, a laser sheet smoke visualization study of the flow patterns provided a greater understanding of the interaction of the hydrodynamic and thermal boundary layers.

Local Nusselt numbers were calculated from the non-dimensional temperature gradients along the heated walls multiplied by the ratio of the fluid thermal conductivity at the hot and cold surface, respectively

$$Nu(\zeta) = \left[\frac{K_H}{K_C}\frac{\partial(T-T_C)/(T_H-T_C)}{\partial(x/H)}\right]_s. \quad (8)$$

The mean Nusselt number was determined by

$$\overline{Nu} = \int_0^1 Nu(\zeta)\,d\zeta. \quad (9)$$

The errors in estimating the temperature gradient along the isothermal walls are within $\pm 3\%$ and the total possible error is of the order of $\pm 6\%$. Detailed error and interferogram analyses are given in ref. [26].

Finally, the requirements to obtain steady-state conditions were set as follows. First, the experiment was operated for at least 4 h. Then it was very essential to verify that: (a) thermocouple variations are no more than 0.1°C for at least a time span of 15 min, (b) temperature difference variations of the hot and cold walls are not to exceed 0.05°C over a span of 15 min.

RESULTS AND DISCUSSION

Mean Nusselt number

Figure 3 presents a comparison of the present experimental and numerical mean Nusselt numbers as a function of Rayleigh number for the 90° (vertical) enclosure with previous experimental and numerical calculations. It is important to observe the difference resulting from the assumption of adiabatic walls and the results from the experimental insulated boundary conditions. The calculations of Zhong *et al.* [18] were within 3% with the present results when experimental insulated boundary conditions based on the experiments of Bajorek and Lloyd [27] were incorporated in their numerical scheme. On the other hand, for adiabatic boundary conditions the Nusselt number is over-estimated, due to the suppression of conduction effects near the end walls. The experimental results of Bajorek and Lloyd [27] exhibited excellent agreement with the present data. For the experimental data presented here, the correlation of the mean Nusselt number for the vertical (90°) enclosure orientation as a function of Rayleigh number is found to be

$$\overline{Nu} = 0.175Ra^{0.275}. \quad (10)$$

This equation correlated the data with a maximum deviation of $\pm 3\%$ over a Rayleigh number range of 10^4–10^6.

The influence of inclination on the mean Nusselt number for a variety of Rayleigh numbers is displayed in Fig. 4. Results of different numerical and experimental investigations together with the present experimental and numerical results are presented. It is quite clear from the data that an increase of the angle of inclination from 0° (heated from above), causes an increase in the heat transfer which is due to the increase in the driving potential for natural convection. An increase of the inclination angle beyond 90°

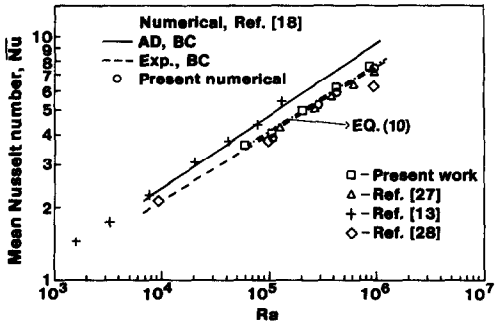

FIG. 3. Comparison of mean Nusselt number results, at $\phi = 90°$ and $A_x = 1.0$.

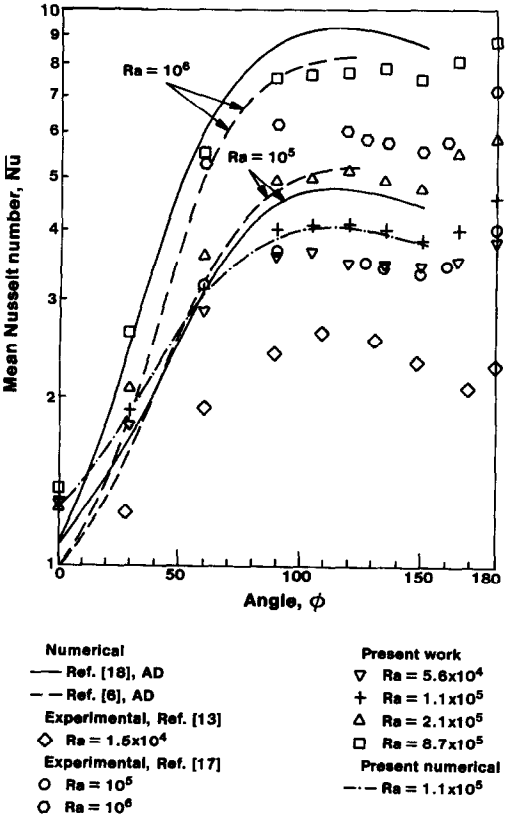

FIG. 4. Effect of inclination angle on mean Nusselt number, at $A_x = 1.0$.

will reduce the gravity component along the heated wall, although the heat transfer rate continues to increase until a maximum value is reached at an angle between 110° and 120°. Beyond this point an increase in the angle will result in a decrease of the average heat transfer until a local minimum is obtained between 150° and 160°. The heat transfer then increases reaching a weak maximum value at 180°. The minimum occurs when the flow exhibits a transition from longitudinal rolls to a three-dimensional cellular flow configuration. It is noted that for angles between 0° and 150° and for $Ra = 1.1 \times 10^5$ the agreement between the experiments and the numerical results using the experimental boundary conditions is very good. In the present study the numerical scheme became unstable at an inclination angle greater than 150°.

On the whole, the present results showed excellent agreement with the experimental results of Arnold *et al.* [17]. Their prediction of the local minimum is at 155° for an aspect ratio of one, and a Rayleigh number between 5×10^4 and 10^7 rather than at 175° as predicted by the experiments of Ozoe *et al.* for a Rayleigh number of 1.5×10^4 and an aspect ratio of one [13]. This shift of the local minimum toward the horizontal (180°) is presumably a function of the low Rayleigh number. Also, shown are the numerical results of Zhong *et al.* [18] and Catton *et al.* [6] for inclination angles up to 150°. Their numerical schemes became unstable at an inclination angle greater than 150°. As a result of a detailed examination of all the data, the following correlations were recommended [17, 18].

For $150° < \phi \leqslant 180°$

$$\overline{Nu}(\phi) = \overline{Nu}(180)(\cos(\phi - 180)). \quad (11)$$

For $\phi \leqslant 150°$

$$\overline{Nu}(\phi) = [\overline{Nu}(90) - \overline{Nu}(0)][2/\pi\phi \sin(\phi)] + \overline{Nu}(0). \quad (12)$$

These equations predicted the experimental data within ±10% over $10^4 < Ra \leqslant 10^6$.

Local Nusselt number

The distribution of local Nusselt numbers will be presented along the hot and cold surfaces as a function of the non-dimensional enclosure height, and the angle of inclination between 0° and 180°. A series of

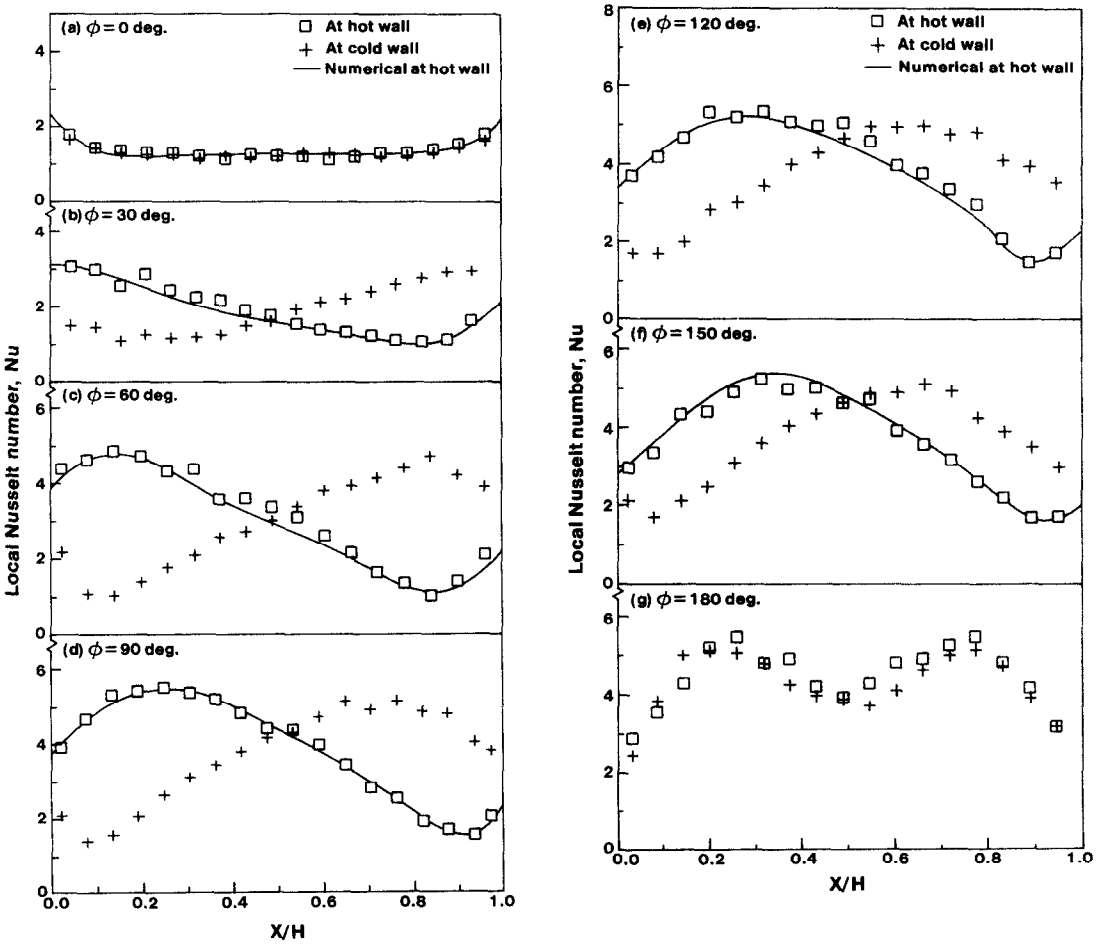

FIG. 5. Effect of inclination angle on local Nusselt number along the hot and cold walls, at $A_x = 1.0$ and $Ra = 1.1 \times 10^5$: (a) $\phi = 0°$; (b) $\phi = 30°$; (c) $\phi = 60°$; (d) $\phi = 90°$; (e) $\phi = 120°$; (f) $\phi = 150°$; (g) $\phi = 180°$.

interferograms, flow visualizations, and numerically predicted stream functions and isotherms are shown to provide additional qualitative understanding of the local heat transfer data.

Figure 5(a) shows the local variations of heat transfer distribution at 0° (heated from above) for $Ra = 1.1 \times 10^5$. The local values are almost equal to one as a consequence of pure conduction between the differentially heated walls except near the corners where the heat transfer increases. This is evidence of a combination of convective flow and conduction to the insulated walls. Figures 6(a) and 7(a) indicate this convective nature near the corners, however, the flow is extremely slow because of the gravitationally stable condition. Moreover, the isotherms bending near the end walls as shown in Figs. 8(a) and 9(a) depict the existence of some variation in heat transfer. Another point to consider from the isotherms is the fact that they reflect the thermal boundary layer configuration in the immediate vicinity of the heated walls. Thus a qualitative picture of the local heat transfer rate can be obtained which is related to the inverse of the thermal boundary layer thickness.

For inclination angles of 30° and 60° the convective flow is very evident as shown in Figs. 6(b), (c) and 7(b), (c). At 30° the flow is confined to the boundary layer, however at 60° the driving potential of the convective flow influences the core region as illustrated experimentally and numerically in Figs. 6(c) and 7(c). This fact is clear from the appearance of two symmetrical vortical tubes that reside near the centers of the isothermal walls. In this event, the patterns of the isotherms, Figs. 8(b) and (c) illustrate the corresponding development of the thermal boundary layer, which is in excellent agreement with the numerical results in Figs. 9(b) and (c). Also, the thickness of the thermal boundary layer seems to be strongly dependent on the angle of inclination and corresponds to an increase of the convective flow. For inclination angles of 30° and 60° the local heat transfer distributions are shown in Figs. 5(b) and (c). It is clear that the convective flow. For inclination angles of 30°

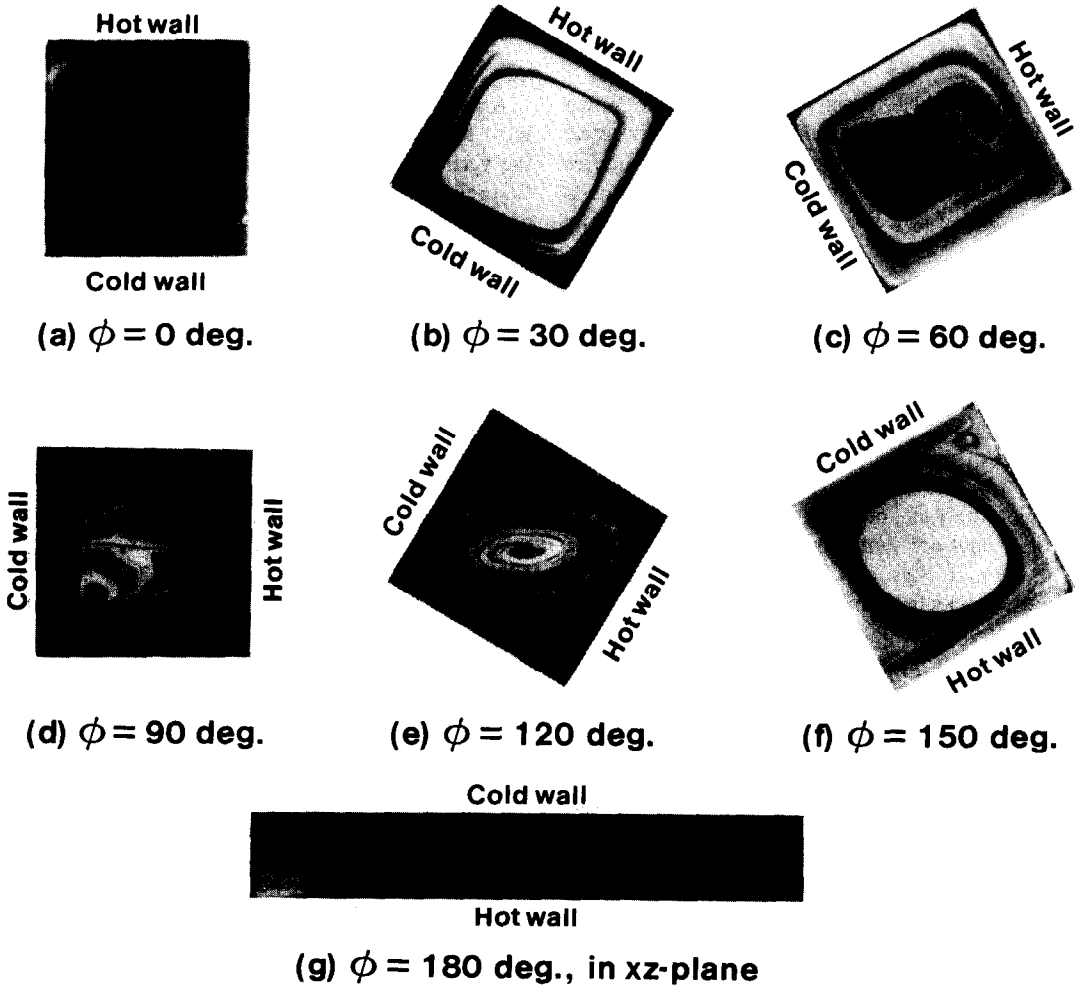

FIG. 6. Flow pattern in x–y plane, at $Ra = 3.0 \times 10^5$: (a) $\phi = 0°$; (b) $\phi = 30°$; (c) $\phi = 60°$; (d) $\phi = 90°$; (e) $\phi = 120°$; (f) $\phi = 150°$; (g) $\phi = 180°$, in x–z plane.

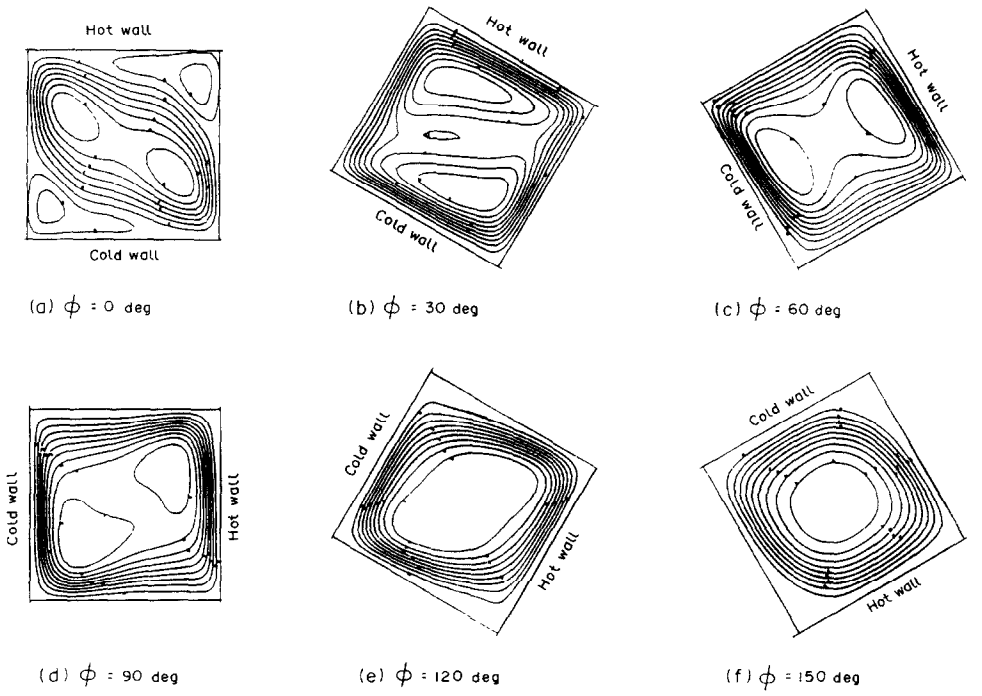

FIG. 7. Stream function in x–y plane, at $Ra = 3.0 \times 10^5$: (a) $\phi = 0°$; (b) $\phi = 30°$; (c) $\phi = 60°$; (d) $\phi = 90°$; (e) $\phi = 120°$; (f) $\phi = 150°$.

and 60° the local heat transfer distributions are shown in Figs. 5(b) and (c). It is clear that the convective flows grow in strength as the angle increases. Figures 6(b) and 7(b) show the experimentally and numerically determined flow fields for 30°. It is seen that the flow is more of a boundary layer type at the walls and that the central core region is dominated by a slow moving stratified cellular pattern. The isothermal plots of Figs. 8(b) and 9(b) confirm the existence of the stratified temperature field which indicates that conduction is a dominant mode of heat transfer.

At 60° the local heat transfer increases and clear maxima and minima are observed at about $0.17H$ from the top and bottom corners. The heat transfer profiles of the hot and cold surfaces are similar to each other and are symmetric about $x/H = 0.5$. The flow patterns in Figs. 6(c) and 7(c) both indicate the flow pattern which is similar about the central plane. The isotherm fringe patterns from the interferometer are not as stratified as those predicted in the numerical study, but this is not considered very significant. Clearly convection is much stronger than at 30°.

At 90° a skewness is observed in the experimental and numerical local heat transfer rates in Fig. 5(d). Also the overall value of the heat transfer increases. These observations are a result of a movement of the vortices to more of a 'downstream' location, as seen in Figs. 6(d) and 7(d), because of the increase in the magnitude of the gravity vector along the vertical surface of the enclosure. The body force exerted on the fluid is greater and the flow velocity increases yielding a stronger convective flow. The hot and cold wall profiles basically remain mirror images.

A comparison of the experimental and numerical local heat transfer distribution on the hot wall for the vertical enclosure with the experimental data of Bajorek and Lloyd [27] and numerical predictions for perfectly conducting and adiabatic walls of Catton *et al.* [6] is given in Fig. 10. Although the trends of the numerical predictions of ref. [6] are similar in the mid-height regions to the experimental data, the difference is very apparent near the end walls. Figure 11 presents another comparison of local Nusselt number variations from various experimental and numerical results. In general terms the experimental data of ref. [27] are in excellent agreement with the present results. However, the numerical predictions of refs. [29, 30] after assuming similar local Nusselt number variations along the hot wall, do not agree with the experimental data or even with each other. This is partially a result of the different grid sizes and the calculation schemes used in their numerical analyses, but the difference in the insulated wall boundary condition between the experiments and all numerical predictions except for the present calculations is the basic reason for disagreement.

Although further increase of the inclination angle to 120° and 150° does relatively little to the local heat transfer distributions seen in Figs. 5(e) and (f), the flow pattern is changing significantly. Figures 6(e), (f) and 7(e), (f) present the flow structure and stream function at 120° and 150°. They are dominated by a single roll cell oriented with the longitudinal axis of the enclosure (z-axis). At 120° the appearance of a weak secondary flow in the region near the upper and opposite lower corners of the enclosure is observed.

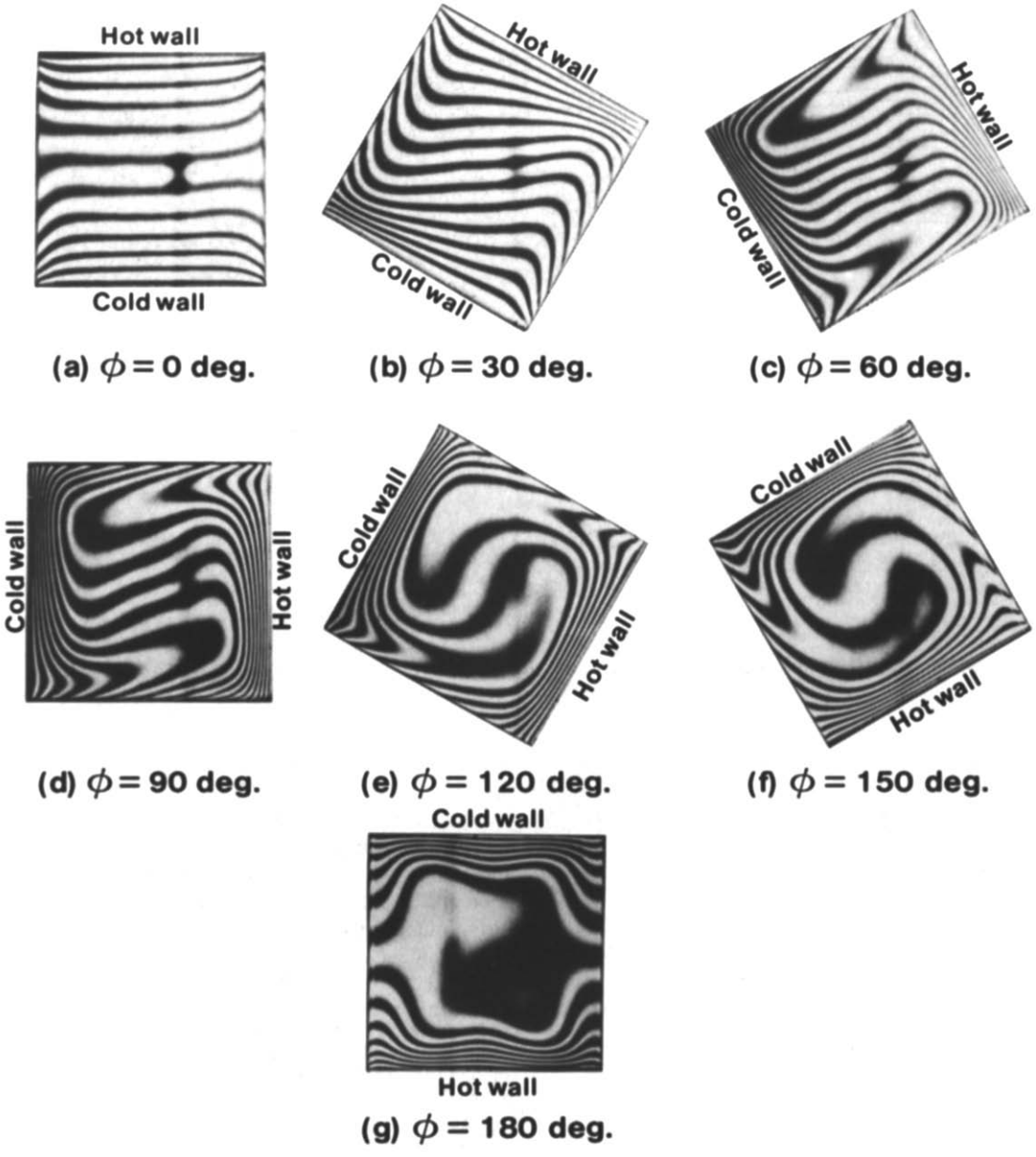

FIG. 8. Interference fringe patterns of isotherms, at $Ra = 1.1 \times 10^5$: (a) $\phi = 0°$; (b) $\phi = 30°$; (c) $\phi = 60°$; (d) $\phi = 90°$; (e) $\phi = 120°$; (f) $\phi = 150°$; (g) $\phi = 180°$.

At 150°, Fig. 6(f), the dominant central roll cell is nearly in a circular form and the secondary flows in the outer regions are more well defined. These weak vortices are responsible for the observed reduction in the overall heat transfer rate.

The onset of cellular convection at 180° is shown in Fig. 6(g) where the flow is aligned in a series of roll cells normal to the isothermal walls. The subsequent unstable temperature field is displayed in Fig. 8(g). It is interesting to note from the isotherm structure the linear temperature distributions along the insulated walls, while the core region remains nearly at a uniform temperature. Measurements of the local Nusselt number presented in Fig. 5(g) indicate the existence of two maximum values in the local heat transfer, which is in a good qualitative agreement with Fig. 8(g).

CONCLUSIONS

The present study has presented for the first time a complete set of matched experimental and numerical data showing the influence of inclination on the local Nusselt number distribution in the enclosure, and has underlined the significance of the need to match numerical boundary conditions to those used in the experiments. In addition, the visual study of the flow motion and the patterns of the isotherms along with

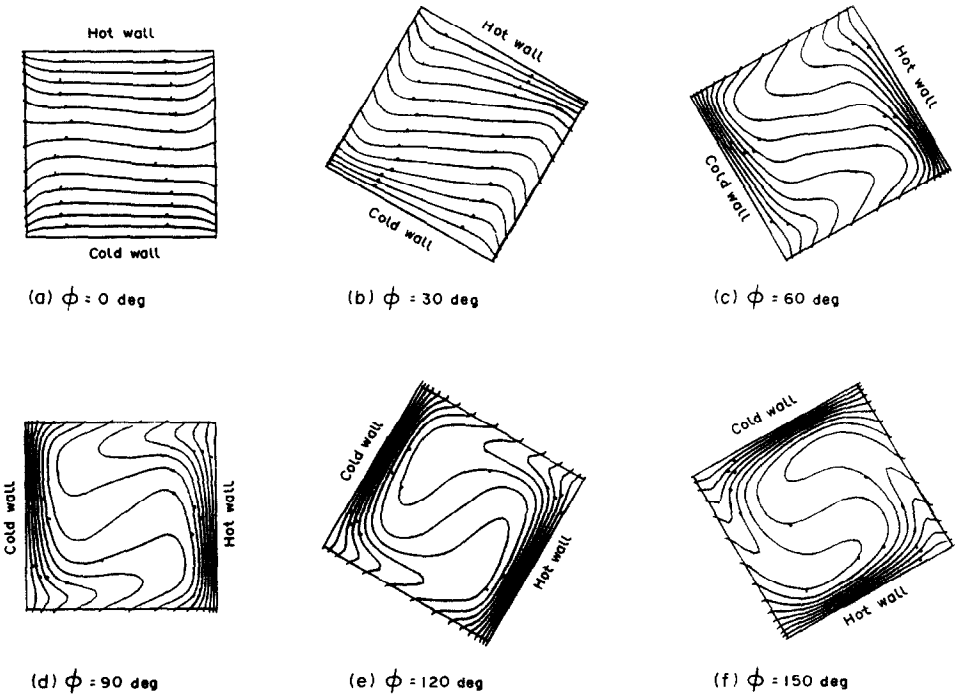

FIG. 9. Isotherms, at $Ra = 1.1 \times 10^5$: (a) $\phi = 0°$; (b) $\phi = 30°$; (c) $\phi = 60°$; (d) $\phi = 90°$; (e) $\phi = 120°$; (f) $\phi = 150°$.

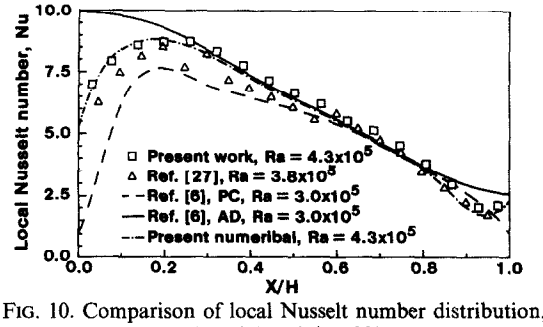

FIG. 10. Comparison of local Nusselt number distribution, at $A_x = 1.0$ and $\phi = 90°$.

the stream functions and the isotherms have added greatly to the physical understanding of the hydrodynamic and thermal boundary layer interaction at different angles of inclination. In this respect, it was suggested that, even for a gravitationally stable condition at 0° (heated from above) the local values of the heat transfer rate are different from unity near the corners due to the existence of convective flows, which come from the insulated side walls. The experimental and numerical results presented herein are in very good agreement and constitute an excellent reference for all numerical and analytical studies on local heat transfer in enclosures.

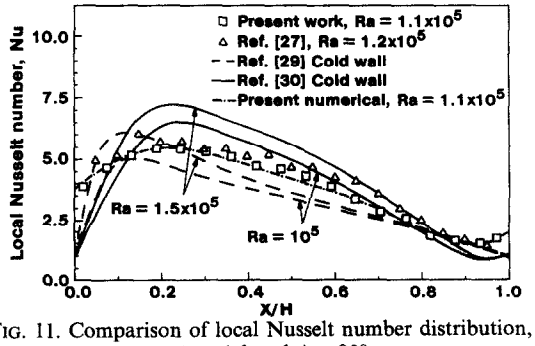

FIG. 11. Comparison of local Nusselt number distribution, at $A_x = 1.0$ and $\phi = 90°$.

Acknowledgement—The authors would like to express their gratitude for the support of the National Science Foundation Grant CBT 82-19158, as well to Michigan State University and the University of Notre Dame for the use of their computing facilities.

REFERENCES

1. S. Ostrach, Natural convection in enclosures. In *Advances in Heat Transfer* (Edited by J. P. Hartnett and T. F. Irvine, Jr.), Vol. 8, pp. 161–227. Academic Press, New York (1972).
2. I. Catton, Natural convection in enclosures, *Proc. Sixth Int. Heat Transfer Conf.*, Vol. 6, pp. 13–31 (1978).
3. G. D. Raithby and K. G. T. Hollands, *Handbook of Heat Transfer Fundamentals* (Edited by W. M. Rohsenow, J. P. Hartnett and E. N. Ganic), 2nd Edn. McGraw-Hill, New York (1985).
4. J. E. Hart, Stability of the flow in a differentially heated inclined box, *J. Fluid Mech.* **47**, 547–576 (1971).
5. P. S. Ayyaswamy and I. Catton, The Boundary-layer regime for natural convection in a differentially heated, tilted rectangular cavity, *J. Heat Transfer* **95**, 543–545 (1973).
6. I. Catton, P. S. Ayyaswamy and R. M. Clever, Natural convections flow in a finite rectangular slot arbitrarily oriented with respect to the gravity vector, *Int. J. Heat Mass Transfer* **17**, 173–184 (1974).

7. K. G. T. Hollands and L. Konicek, Experimental study of the stability of differentially heated inclined air layers, *Int. J. Heat Mass Transfer* **16**, 1467–1476 (1973).
8. K. G. T. Hollands, Natural convection in horizontal thin-walled honeycomb panels, *J. Heat Transfer* **95**, 439–444 (1973).
9. T. E. Unny, Thermal instability in differentially heated inclined fluid layers, *J. Appl. Mech.* **39**, 41–46 (1972).
10. K. G. T. Hollands, T. E. Unny, G. D. Raithby and L. Konicek, Free convection heat transfer across inclined air layers, *J. Heat Transfer* **98**, 189–193 (1976).
11. S. M. Elshirbiny, G. D. Raithby and K. G. T. Hollands, Heat transfer by natural convection across vertical and inclined air layers, *J. Heat Transfer* **104**, 96–102 (1982).
12. S. M. Elshirbiny, K. G. T. Hollands and G. D. Raithby, Nusselt number distribution in vertical and inclined air layers, *J. Heat Transfer* **105**, 406–408 (1983).
13. H. Ozoe, H. Sayama and S. W. Churchill, Natural convection in an inclined rectangular channel at various aspect ratios and angles—experimental measurements, *Int. J. Heat Mass Transfer* **18**, 1425–1431 (1975).
14. H. Ozoe, H. Sayama and S. W. Churchill, Natural convection in an inclined square channel, *Int. J. Heat Mass Transfer* **17**, 401–406 (1974).
15. H. Ozoe, K. Yamamoto, H. Sayama and S. W. Churchill, Natural circulation in an inclined rectangular channel heated on one side and cooled on the opposing side, *Int. J. Heat Mass Transfer* **17**, 1209–1217 (1974).
16. H. Ozoe, K. Fujii, N. Lior and S. W. Churchill, Long rolls generated by natural convection in an inclined rectangular enclosure, *Int. J. Heat Mass Transfer* **26**, 1427–1438 (1983).
17. J. N. Arnold, I. Catton and D. K. Edwards, Experimental investigation of natural convection in inclined rectangular regions of differing aspect ratios, *J. Heat Transfer* **98**, 67–71 (1976).
18. Z. Y. Zhong, K. T. Yang and J. R. Lloyd, Variable property natural convection in tilted cavities with thermal radiation. In *Numerical Methods in Heat Transfer* (Edited by R. W. Lewis and V. T. Morgan), Vol. 3, pp. 195–214. Wiley, Chichester (1985).
19. H. Q. Yang, K. T. Yang and J. R. Lloyd, Flow transition in laminar buoyant flow in a three-dimensional tilted rectangular enclosure, *Proc. 8th Int. Heat Transfer Conf.*, San Francisco, California, Vol. 4, pp. 1495–1500 (1986).
20. C. J. Chen and V. Talaie, Finite analytic numerical solutions of laminar natural convection in two-dimensional inclined rectangular enclosures, ASME Paper 85-HT-10 (1985).
21. C. S. Reddy, Numerical simulation of laminar natural convection in shallow inclined enclosures, *Proc. Seventh Int. Heat Transfer Conf.*, Vol. 2, pp. 263–268, NC24 (1982).
23. J. G. Symons and M. K. Peck, Natural convection heat transfer through inclined longitudinal slots, *J. Heat Transfer* **106**, 824–829 (1984).
24. B. P. Leonard, A convective stable, third-order accurate finite-difference method for steady two-dimensional flow and heat transfer. In *Numerical Properties and Methodologies in Heat Transfer* (Edited by T. M. Shih), pp. 221–226. Hemisphere, Washington, DC (1983).
25. H. Q. Yang, Physics-based grid generation for three-dimensional laminar buoyant flow in rectangular enclosure, Ph.D. thesis, University of Notre Dame, Notre Dame, Indiana (1986).
26. F. J. Hamady, Experimental study of local natural convection heat transfer in inclined and rotating enclosures, Ph.D. thesis, Michigan State University, East Lansing, Michigan (1987).
27. S. M. Bajorek and J. R. Lloyd, Experimental investigation of natural convection in partitioned enclosures, *J. Heat Transfer* **104**, 527–532 (1982).
28. W. M. M. Schinkel, S. J. M. Linthorst and C. J. Hoogendooen, The stratification in natural convection in vertical enclosures, *J. Heat Transfer* **105**, 267–272 (1983).
29. F. Bauman, A. Gadgil, R. Kammerud and R. Greif, Buoyancy-driven convection in rectangular enclosures: experimental results and numerical calculations, ASME Publication 80-HT-66 (1980).
30. G. De Vahl Davis, Laminar natural convection in an enclosed rectangular cavity, *Int. J. Heat Mass Transfer* **11**, 1675–1693 (1968).

ETUDE DU TRANSFERT LOCAL DE CHALEUR PAR CONVECTION NATURELLE DANS UNE ENCEINTE FERMEE

Résumé—On étudie expérimentalement et numériquement l'effet de l'inclinaison sur les caractéristiques locales du transfert thermique en convection naturelle stationnaire dans une enceinte emplie d'air, différemment chauffée, avec un rapport de forme de section droite. Des mesures des nombres de Nusselt locaux et globaux sont réalisées pour différents angles d'inclinaison entre 0° (chauffage par dessus) et 180° (chauffage par dessous), pour des nombre de Rayleigh entre 10^4 et 10^6, et sont comparées aux prédictions numériques. Le flux thermique sur les frontières chaude et froide montre une forte dépendance vis-à-vis de l'angle d'inclinaison et du nombre de Rayleigh. En outre, on présente de nouveaux résultats ou des détails sur les distributions du transfert thermique local en fonction de l'angle d'inclinaison et du nombre de Rayleigh. Les configurations d'écoulement, les fonctions de courant et les isothermes pour différents angles d'inclinaison sont fournies de façon à donner une nouvelle et meilleure compréhension de l'écoulement et du transfert de chaleur.

UNTERSUCHUNG DES ÖRTLICHEN WÄRMEÜBERGANGS BEI NATÜRLICHER KONVEKTION IN EINEM GENEIGTEN HOHLRAUM

Zusammenfassung—Der Einfluß der Neigung auf den örtlichen Wärmeübergang bei stationärer natürlicher Konvektion in einem unterschiedlich beheizten Hohlraum wurde theoretisch und experimentall untersucht. Der Hohlraum ist mit Luft gefüllt und besitzt ein Seitenverhältnis von 1. Die örtliche und die mittlere Nusselt-Zahl wurden bei Neigungswinkeln zwischen 0° (von oben beheizt) und 180° (von unten beheizt) gemessen und mit den numerisch vorausberechneten Werten verglichen. Die Rayleigh-Zahl betrug dabei zwischen 10^4 und 10^6. Die Wärmeströme an den kalten und heißen Grenzflächen hängen stark von Neigungswinkel und Rayleigh-Zahl ab. Zusätzlich werden neue Ergebnisse und Einzelheiten über den örtlichen Wärmeübergang als Funktion von Neigungswinkel und Rayleigh-Zahl vorgestellt. Strömungsbilder, Stromfunktionen und Isothermen werden für verschiedene Neigungswinkel gezeigt, um ein besseres und tieferes Verständnis der Strömungs- und Wärmeübertragungsvorgänge zu ermöglichen.

ИССЛЕДОВАНИЕ ЛОКАЛЬНЫХ ХАРАКТЕРИСТИК ТЕПЛОПЕРЕНОСА ПРИ ЕСТЕСТВЕННОЙ КОНВЕКЦИИ В НАКЛОННОЙ ПОЛОСТИ

Аннотация—Экспериментально и численно исследуется влияние наклона на локальные характеристики теплопереноса при стационарной естественной конвекции в заполненной воздухом неравномерно нагретой полости в зависимости от отношения характерных размеров полости. Результаты измерений локальных и средних чисел Нуссельта при изменении угла наклона полости от 0° (нагрев сверху) до 180° (нагрев снизу) в диапазоне чисел Рэлея 10^4–10^6 сравниваются с численными прогнозами. Обнаружена сильная зависимость величины теплового потока на горячей и холодной стенках от угла наклона и числа Рэлея. Кроме того, приведены новые результаты и уточнены известные данные о зависимости локальных характеристик теплопереноса от угла наклона и числа Рэлея. Приведенные структуры потоков, функции тока и изотермы позволяют по-новому взглянуть на характер течения и теплопереноса и глубже понять природу изучаемых процессов.